A frequency-domain thermoreflectance method for the characterization of thermal properties

Aaron J. Schmidt, Ramez Cheaito, and Matteo Chiesa

View Online   Export Citation

ARTICLES YOU MAY BE INTERESTED IN

A frequency-domain thermoreflectance method for the characterization of thermal properties

Aaron J. Schmidt,[1,a)] Ramez Cheaito,[2] and Matteo Chiesa[2]

[1]*Department of Mechanical Engineering, Massachusetts Institute of Technology, Cambridge, Massachusetts 02139, USA and Department of Mechanical Engineering, Masdar Institute of Science and Technology, Abu Dhabi, United Arab Emirates*
[2]*Department of Mechanical Engineering, Masdar Institute of Science and Technology, Abu Dhabi, United Arab Emirates*

A frequency-domain thermoreflectance method for measuring the thermal properties of homogenous materials and submicron thin films is described. The method can simultaneously determine the thermal conductivity and heat capacity of a sample, provided the thermal diffusivity is $\gtrsim 3 \times 10^{-6}$ m^2/s, and can also simultaneously measure in-plane and cross-plane thermal conductivities, as well the thermal boundary conductance between material layers. Two implementations are discussed, one based on an ultrafast pulsed laser system and one based on continuous-wave lasers. The theory of the method and an analysis of its sensitivity to various thermal properties are given, along with results from measurements of several standard materials over a wide range of thermal diffusivities. We obtain specific heats and thermal conductivities in good agreement with literature values, and also obtain the in-plane and cross-plane thermal conductivities for crystalline quartz. © *2009 American Institute of Physics.* [doi:10.1063/1.3212673]

I. INTRODUCTION

Interest in the thermal properties of thin films has led to the development of many noncontact measurement techniques based on photothermal phenomena. These can be roughly grouped into frequency-domain methods based on a modulated laser heating source[1–9] and time-domain methods based on the time delay between pulses from a pulsed laser heating source, commonly called time-domain thermoreflectance (TDTR).[10–13] Advantages of the TDTR method include good sensitivity to thermal interfaces and conductivities of submicron thin films, and a straightforward laser spot geometry that leads to convenient data analysis. On the other hand, frequency-domain methods avoid the complexity associated with a mechanical delay stage and the high cost of a pulsed laser system.

In this work, we present a frequency-domain thermoreflectance (FDTR) method that combines the advantages of TDTR with the relative experimental simplicity of modulated photothermal methods. This is accomplished by using the same spot geometry and analysis approach as TDTR, while making frequency instead of time delay the independent experimental parameter. By varying the modulation frequency over a wide range (maximum 25 kHz–20 MHz), we obtain a frequency-domain measurement that yields the same parameters as TDTR with similar or improved sensitivity, including the thermal conductivity of homogenous materials and films in the submicron range and the thermal boundary conductance between layers. In addition, for samples with a thermal diffusivity $\gtrsim 3 \times 10^{-6}$ m^2/s, FDTR can reliably extract thermal conductivity, boundary conductance, and the

volumetric heat capacity of a sample simultaneously. Alternatively, a single measurement can yield both the in-plane and cross-plane thermal conductivities of a sample. The FDTR method can be implemented with an ultrafast pulsed laser system, allowing easy switching between FDTR and TDTR, or with continuous-wave (cw) lasers, allowing for a simpler, less expensive system without a mechanical delay stage.

We present the theory of the FDTR method for both cw and pulsed laser systems, and an analysis of its sensitivity to various thermal properties. We describe our particular implementation, based on an ultrafast pulsed Ti:sapphire system and demonstrate results from standard materials over a wide range of thermal diffusivities. Finally, we obtain specific heats and thermal conductivities in good agreement with literature values and also obtain both in-plane and cross-plane thermal conductivities for crystalline quartz.

II. EXPERIMENTAL SETUP

Two possible experimental setups for FDTR are shown in Fig. 1. The first, in Fig. 1(a), is based on cw lasers. One laser passes through an electro-optic modulator (EOM) driven by a function generator and provides the modulated heating source. A lock-in amplifier records the amplitude and phase response of the reflected probe beam to the thermal wave, and these quantities are related back to the properties of the sample. In our method, we use the phase of the probe beam as the observable quantity since the amplitude at each frequency is affected by the frequency response of the detector and measurement cables.

The detector, the cables, the instruments, and the different optical path lengths taken by the beams also introduce a

---

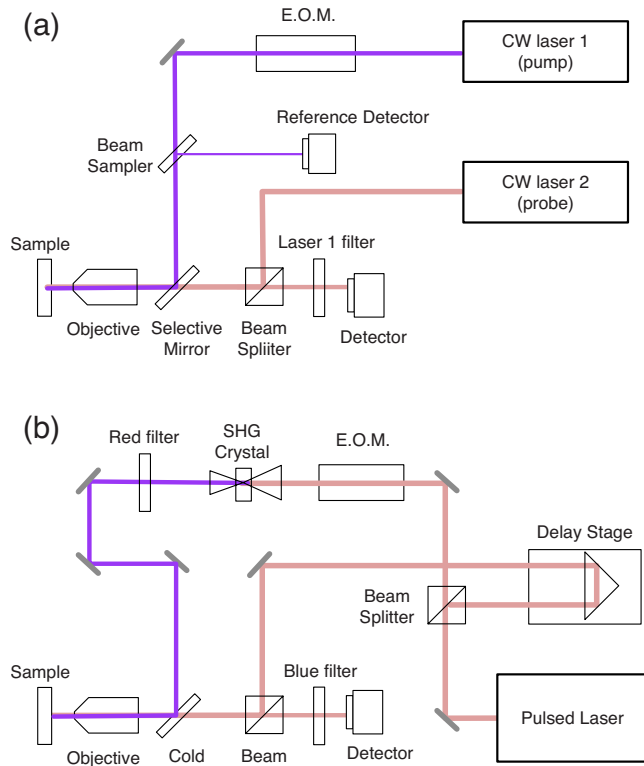a)Electronic mail: aarons@alum.mit.edu.

FIG. 1. (Color online) Two possible experimental arrangements for FDTR. (a) A system based on cw lasers. Laser 1 (the pump laser) is passed through an EOM and provides the modulated heat source, while laser 2 (the probe laser) measures the thermoreflectance signal. Both beams are directed co-axially through a single objective lens onto the sample. A matched reference detector is used to determine the true phase of laser 1 at the sample. (b) A system based on a pulsed laser. Each pulse is split into pump and probe pulses. Probe pulses are delayed relative to the pump pulses with a mechanical stage. The pump beam passes through an EOM and a second harmonic generation crystal before being directed onto the sample.

frequency-dependent phase shift into the measured signal. In order to determine the true phase of the pump laser imping-ing on the sample, a portion of the pump light after the EOM can be split off and sent to a reference photodetector that is identical to the primary photodetector. The reference photo-detector serves as the reference for the lock-in amplifier. The optical path length between the reference detector and the EOM should be made equal to the sum of the path length between the EOM and the sample and the path length be-tween the sample and the probe detector. The error intro-duced by path mismatch scales linearly with frequency; at 10 MHz modulation, a 1 cm difference in optical paths trans-lates to a phase error of roughly 0.1°.

The second setup, shown in Fig. 1(b), is based on a pulsed laser and is similar to setups commonly used for TDTR. This is the arrangement we have used to generate all the data presented in this work. A Ti-sapphire laser emits a train of 150 fs long pulses at a repetition rate of 80 MHz. The center wavelength is 815 nm and the power per pulse is roughly 15 nJ. Each pulse is split into pump and probe pulses, and the probe pulses are delayed relative to the pump pulses with a mechanical stage. The pump beam passes through an EOM and bismuth triborate crystal that doubles the pump light frequency. Dielectric mirrors and color filters

isolate the pump beam from the detector, allowing us to mea-sure relatively rough samples since the filters are not affected by scattering of the pump beam into different polarizations and angles. More details on our setup are given elsewhere.[14]

Due to the high pulse repetition rate of the Ti-sapphire laser, in thermal measurements there is not sufficient time for the sample to return to equilibrium between laser pulses, and this ultimately introduces a thermal wave into the sample at the EOM modulation frequency.[12,15,16] Like in the cw sys-tem, a lock-in amplifier records the amplitude and phase re-sponse of this thermal wave, and these quantities are related to the properties of the sample. In this setup, the reference detector approach can also be used to determine the pump beam phase, although a sharp low-pass filter would be needed to remove the harmonic response at the laser pulsing frequency. An alternative method is to adjust the phase of the lock-in at each frequency until the out-of-phase component of the signal is constant as the stage moves across the zero-delay time.[12] This is the approach we employ in our system. The phase correction can be determined once over the range of modulation frequencies and then automatically added dur-ing subsequent measurements.

III. ANALYSIS

A. Theory

The ideal lock-in amplifier measures the fundamental harmonic component of the probe signal at the modulation frequency ω_0 and rejects all other components. The output is the amplitude A and phase ϕ of the fundamental component of the probe signal with respect to the reference wave. Math-ematically, the solution can be expressed as a complex num-ber $Z(\omega_0)$ such that the output of the lock-in amplifier for a reference wave $e^{i\omega_0 t}$ is given by

$$A e^{i(\omega_0 t + \phi)} = Z(\omega_0) e^{i\omega_0 t}. \tag{1}$$

In the case of pulsed pump and probe beams[12,15]

$$Z(\omega_0) = \beta \sum_{k=-\infty}^{\infty} H(\omega_0 + k\omega_s) e^{ik\omega_s \tau}, \tag{2}$$

where τ is the delay time between pump and probe pulses, ω_s is the laser pulsing frequency, $H(\omega_0)$ is the thermal frequency response of the sample weighted by the intensity of the probe beam, and β is a factor including the thermoreflectance co-efficient of the sample and the power in the pump and probe beams. This result assumes the sample responds as a linear system and behaves as a continuum; these conditions are usually met for small temperature excursions and delay times greater than ~100 ps.

The weighted sample frequency response, $H(\omega_0)$, is ob-tained by solving the heat diffusion equation for a Gaussian heat source (the pump beam) impinging on a multilayer stack of materials and weighting the resulting temperature distri-bution at the top surface by the Gaussian intensity distribu-tion of the probe beam. A full treatment of this problem can be found elsewhere.[12,15] Here we repeat the essential ele-ments necessary to understand our results.

For a single slab of material in the frequency domain, the temperature θ_t and heat flux f_t on the top side of the slab are related to the temperature θ_b and heat flux f_b on the bottom side through

$$\begin{bmatrix} \theta_b \\ f_b \end{bmatrix} = \begin{bmatrix} \cosh(qd) & \dfrac{-1}{\sigma_z q}\sinh(qd) \\ -\sigma_z q \sinh(qd) & \cosh(qd) \end{bmatrix} \begin{bmatrix} \theta_t \\ f_t \end{bmatrix}. \quad (3)$$

Here d is the layer thickness, σ_z the cross-plane thermal conductivity and

$$q^2 = \frac{\sigma_r k^2 + \rho c i \omega}{\sigma_z}, \quad (4)$$

where ρ is the density, c is the specific heat capacity, and σ_r and σ_z are the radial and cross-plane thermal conductivities, respectively. The heat flux boundary condition at the top layer f_t is given by the Hankel transform of a Gaussian spot with power A_0 and $1/e^2$ radius w_0

$$f_t = \frac{A_0}{2\pi}\exp\left(\frac{-k^2 w_0^2}{8}\right). \quad (5)$$

Multiple layers are handled by multiplying the matrices for individual layers together

$$\begin{bmatrix} \theta_b \\ f_b \end{bmatrix} = \mathbf{M}_n \mathbf{M}_{n-1} \cdots \mathbf{M}_1 \begin{bmatrix} A & B \\ C & D \end{bmatrix} \begin{bmatrix} \theta_t \\ f_t \end{bmatrix}, \quad (6)$$

where $\mathbf{M}_n$ is the matrix for the bottom layer. An interface conductance G is treated by taking the limit as the heat capacity of a layer approaches zero and choosing σ_z and d such that $G = \sigma_z/d$. If the bottom surface of the nth layer is assumed to be adiabatic, or if the nth layer is treated as semi-infinite, then in both cases Eq. (6) reduces to $C\theta_t + Df_t = 0$ and the surface temperature will be given by

$$\theta_t = \frac{-D}{C} f_t. \quad (7)$$

If the thickness of the bottom layer is greater than the thermal penetration depth at the lowest frequency $\sqrt{2\alpha/\omega_0}$, where α is the thermal diffusivity of the layer; then the semi-infinite boundary condition is an accurate description of the physical situation. Otherwise a finite thickness for the final layer must be used in the solution.

The final frequency response $H(\omega)$ in real space is found by taking the inverse Hankel transform of Eq. (7) and weighting the result by the probe intensity distribution, which is taken as a Gaussian spot with $1/e^2$ radius w_1 (Ref. 12)

$$H(\omega) = \frac{A_0}{2\pi}\int_0^\infty k\left(\frac{-D}{C}\right)\exp\left[\frac{-k^2(w_0^2 + w_1^2)}{8}\right]dk. \quad (8)$$

This result is inserted into Eq. (2). The measurement of individual materials physical properties is performed as an inverse problem, minimizing the error between the lock-in phase data and the phase of Eq. (2) via a nonlinear least-squares algorithm. When cw lasers are used instead of a pulsed laser, the thermal analysis is identical but instead of Eq. (2) we have

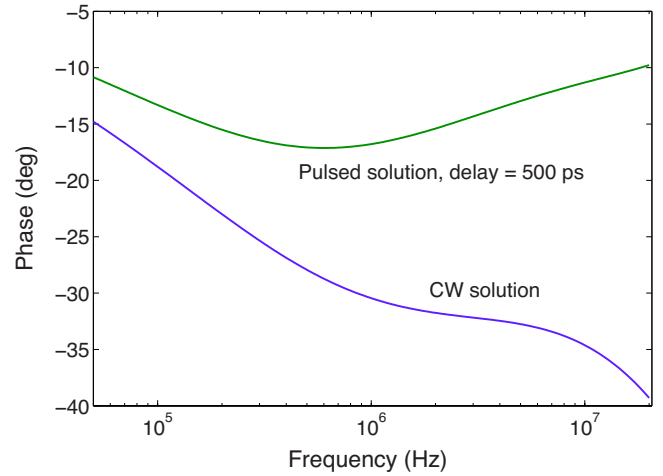$$Z(\omega_0) = \beta H(\omega_0). \quad (9)$$

FIG. 2. (Color online) The calculated phase response for cw and pulsed FDTR measurements of 100 nm of Al on sapphire over the range 50 kHz–20 MHz.

B. Sensitivity analysis

We consider the basic system of a bulk homogenous material coated with 100 nm of Al for sensitivity analysis. Figure 2 shows the calculated phase for an FDTR measurement with sapphire as the substrate. Solutions are shown over a frequency range of 50 kHz–20 MHz for both a pulsed laser system with delay time fixed at $\tau = 500$ ps and the cw solution. We obtain similar results to Fig. 2 for materials over a wide range of thermal diffusivities. The curves have sufficient structure to potentially extract three parameters from the data. Heat transfer in the sample dictates when this is actually possible and is explored later in this section.

We quantify the sensitivity of the phase signal to a parameter x in a manner similar to that of Gundrum *et al.*,[17]

$$S_x = \frac{d\phi}{d\ln x}, \quad (10)$$

where the phase ϕ is in radians. Equation (10) is evaluated for the following substrate parameters: thermal conductivity k, volumetric heat capacity C, and the metal-substrate thermal interface conductance G. All subsequent sensitivity analysis is done for the case of a pulsed FDTR system at a time delay of 500 ps. Similar results are obtained for different delay times and also for the case of the cw system. The pump and probe laser spot radii are both 6 μm $1/e^2$ unless otherwise stated. The results are shown in Fig. 3 for (a) silicon with a thermal diffusivity of 8.9×10^{-5} m^2/s, (b) sapphire with a thermal diffusivity of 1.5×10^{-5} m^2/s, and (c) Pyrex glass with a thermal diffusivity of 7.8×10^{-7} m^2/s.

In the cases of silicon and sapphire, all three sensitivities vary differently over most of the frequency range and it is possible to extract all three of these parameters from a data set. For the case of Pyrex glass, however, the sensitivity to the boundary conductance is low and the sensitivity to the thermal conductivity and heat capacity are very similar over most of the frequency range. The measurement will be insensitive to boundary conductance and only one of the parameters, thermal conductivity or heat capacity can be determined in this case.
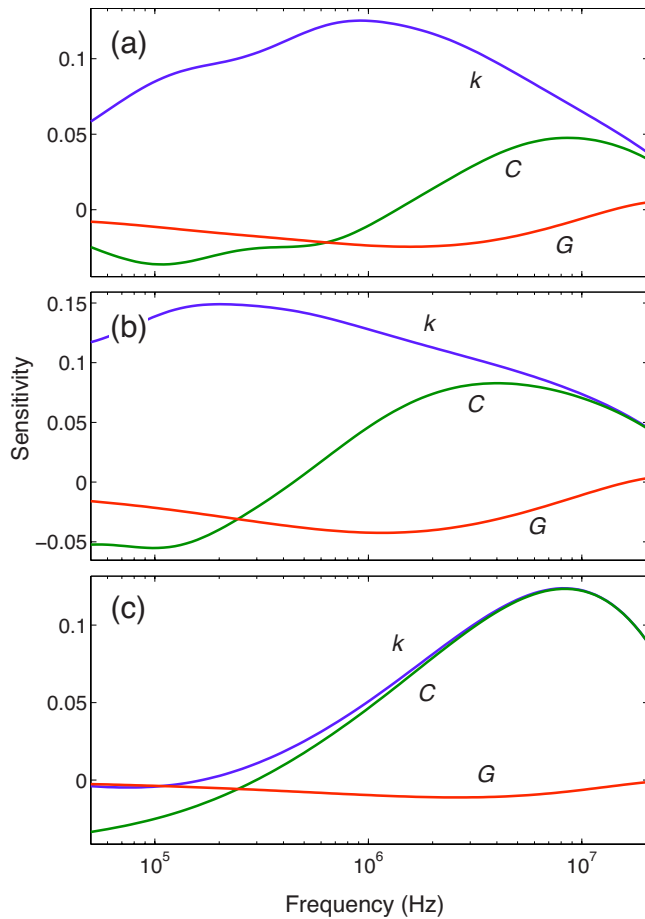
FIG. 3. (Color online) Sensitivity parameter S_x for $x=k$, the substrate thermal conductivity; C, the substrate volumetric heat capacity; and G, the metal-substrate thermal boundary conductance calculated for three substrates: (a) silicon, (b) sapphire, and (c) Pyrex.

FIG. 4. (Color online) Sensitivity parameter S_x for $x=\sigma_z$, the cross-plane thermal conductivity, σ_r, the in-plane thermal conductivity, and G, the metal-substrate thermal boundary conductance, calculated single-crystal quartz.

This latter result is explained by the fact that a different sensitivity to substrate thermal conductivity and heat capacity arises solely from radial heat transport. In the one-dimensional limit, the periodic thermal response depends only on the thermal effusivity of the substrate, $\sqrt{kC}$.[12] This is true for any multilayer system where the substrate layer is semi-infinite. When the thermal penetration depth is much smaller than the laser spot sizes, the periodic response approaches the one-dimensional limit and we cannot determine both k and C of the substrate. This effect is visible in Fig. 3, where at high frequencies, the sensitivities to k and C approach each other. The frequency where they begin to come together depends on the laser spot sizes and thermal penetration depth, which in turn depends on the thermal diffusivity of the substrate and the modulation frequency. We have found that we can reliably determine both substrate thermal conductivity and heat capacity if the difference in sensitivities is $\gtrsim 0.05$ at the bottom of the frequency range. For a frequency range of 25 kHz–20 MHz and laser spot radii on the order of 10 μm, this corresponds to a substrate thermal diffusivity $\gtrsim 3 \times 10^{-6}$ m^2/s. Also, because separation of the sensitivities arises from radial transport, we can only accurately determine both k and C if the substrate is nearly isotropic or has a known anisotropy.

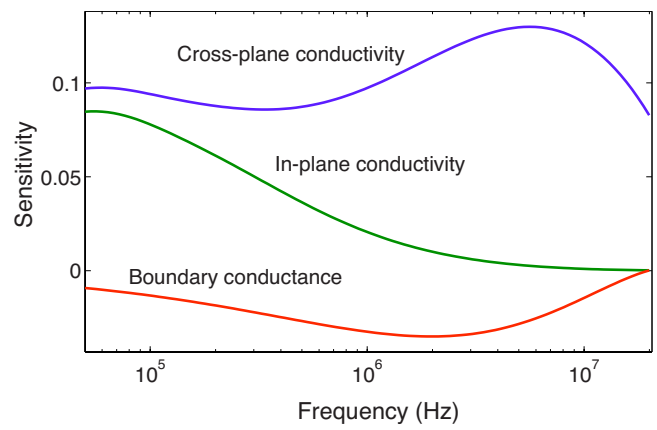Other modulated photothermal methods have been used

to determine both the diffusivity and thermal conductivity of an absorbing film on a known substrate, either by varying the modulation frequency and assuming one-dimensional transport[4] or by scanning the probe spot over the heated region and observing the phase change with probe spot position.[9] Our approach works for an unknown substrate and does not require that the probe spot be scanned across the heated region. We have found that it is also possible to extract both k and C from a single TDTR measurement if the modulation frequency is sufficiently low. However, FDTR is significantly more robust for this purpose because changing frequency regimes has a stronger effect on the sensitivities than changing the delay time between laser pulses at a single frequency. We have found, however, that we can achieve similar results to FDTR by simultaneously fitting TDTR scans from two or more widely spaced frequencies (for example, 0.1, 1, and 10 MHz). This "hybrid" approach may in some cases be more convenient and offers the additional possibility of fitting TDTR measurements at successively lower frequencies to determine the properties of a layered or inhomogenous material at different depths.

We now focus on the sensitivity of the measurement to radial thermal transport. As discussed above, at low frequencies, the thermal penetration depth is comparable to the focused laser spots sizes, typically ~ 10 μm and radial transport becomes a factor. At high frequencies, the measurement approaches a one-dimensional solution and only cross-plane thermal conductivity matters. Previously, it was shown how multiple TDTR measurements at different frequencies could be used to measure anisotropic thermal conductivity.[15] Here, we consider the sensitivity of a single FDTR measurement to anisotropic thermal conductivity.

Figure 4 shows the sensitivity parameter S_x for $x=\sigma_z$, the cross-plane thermal conductivity σ_r, the radial or in-plane thermal conductivity, and G, the metal-substrate thermal boundary conductance, calculated for single-crystal quartz, a material with a thermal conductivity of 10.8 W/mK parallel to the c-axis, taken here as the cross-plane direction, and 6.2 W/mK perpendicular to the c-axis. As expected, sensitivity to the cross-plane thermal conductivity remains significant
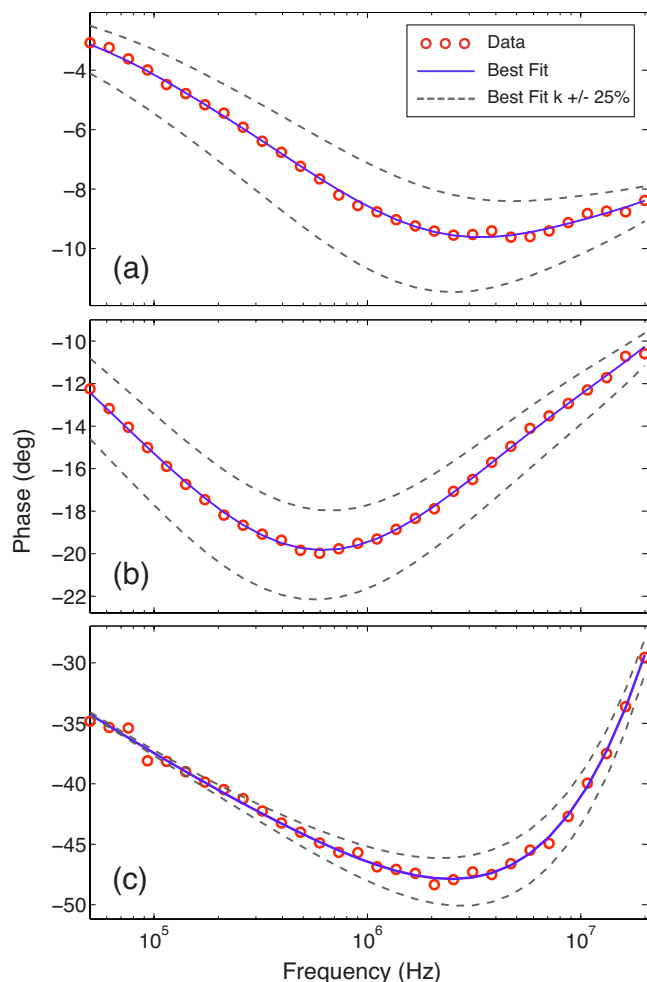
FIG. 5. (Color online) Sample phase data and best-fit curves for three substrates: (a) silicon, (b) sapphire, and (c) Pyrex glass. Also shown are solutions obtained by varying substrate thermal conductivity by ±25%.

TABLE I. Best-fit values obtained from the data in Fig. 5.

Material	k (W/m K)	C (10^6 J/m^3 K)	G (MW/m^2 K)
Silicon	148	1.55	116
Sapphire	40.1	3.09	143
Pyrex	1.34	...	...

accepted literature values.[18,19] The interface conductances are highly dependent on sample surface properties and deposition conditions, but are still in line with previously reported values.[20]

Fitting was performed using a nonlinear least-squares routine, which requires an initial guess to determine the values of the free parameters that minimize the error between the model and data. In order to gauge the robustness of our results, particularly in three-parameter fits, we used several initial guesses and verified that the fitting routine returned the same set of best-fit values. For example, when fitting sapphire, we used the thermal conductivity and heat capacity of silicon, Pyrex and quartz as initial guesses and obtained the same best-fit values in all cases.

In Fig. 6 we show data and the best-fit result for 100 nm of Al on single-crystal quartz with the c-axis parallel to the optical axis. In this case, we are interested in obtaining both the in-plane thermal conductivity σ_r and cross-plane thermal conductivity σ_z, so we choose as our three free parameters σ_z, σ_r/σ_z, and the interface conductance. Best-fit values obtained are 10.6 W/mK for thermal conductivity parallel to the c-axis and 6.5 W/mK perpendicular to the c-axis, both within 10% of accepted values.[18,19] As described above for the previous results, we varied our starting guess values considerably and always converged on the same best-fit values. Dashed lines in Fig. 6 indicate solutions obtained by varying σ_r/σ_z by ±25%. As expected from the sensitivity analysis shown in Fig. 4, the solution is only sensitive to conductivity anisotropy at low frequencies.

across the frequency range, while in-plane thermal conductivity becomes a factor at low frequency. The different natures of the sensitivities make it possible to extract both thermal conductivities from a single measurement as we show in Sec. IV.

IV. SAMPLE RESULTS

Figure 5 shows sample data and best-fit curves for 100 nm of Al on silicon, sapphire, and Pyrex glass. To give a visual indication of the sensitivity, solutions are also shown when the substrate thermal conductivity is varied ±25%. Results obtained by varying heat capacity ±25% have a different shape but are of similar magnitude. These curves are omitted for clarity. For sapphire and silicon samples, both laser spots had a 6 μm $1/e^2$ radius while for the Pyrex sample the pump spot size was doubled to minimize radial conduction in the metal layer. For the sapphire and silicon samples, the free parameters in the fitting were the thermal conductivity of the substrate, volumetric heat capacity of the substrate, and the Al-substrate thermal boundary conductance. For Pyrex, only one of these three, thermal conductivity, was obtained. The best-fit values are summarized in Table I. Conductivities and heat capacities are within 10% of
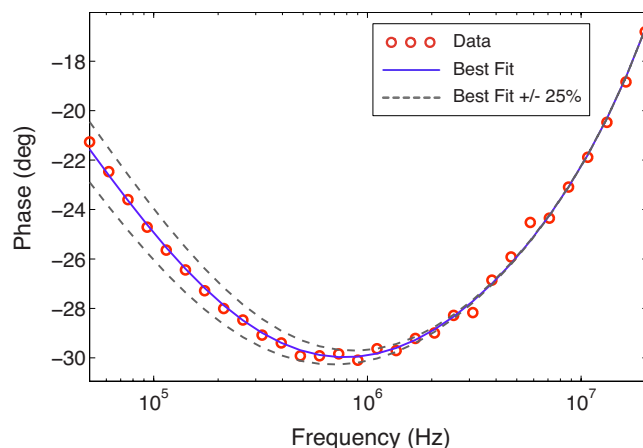

FIG. 6. (Color online) Phase data and best fit for single-crystal quartz with the c-axis parallel to the optical axis. Also shown are solutions obtained by varying ratio of in-plane to cross-plane substrate thermal conductivity by ±25%.
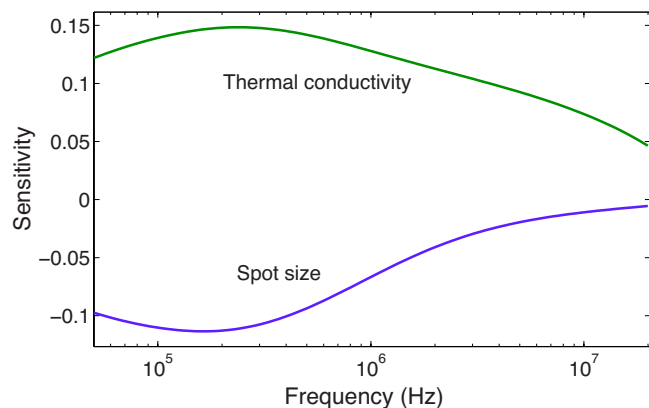
FIG. 7. (Color online) Sensitivity calculation for 100 nm of Al on sapphire for the sensitivity parameters of the pump spot radius and substrate thermal conductivity. Pump and probe spots are taken as having a 6 μm $1/e^2$ radius.

V. SOURCES OF ERROR

Several factors need to be considered to obtain accurate results from an FDTR measurement. The most significant of these is the presence of odd harmonic components of the fundamental frequency in the measured signal, due to the fact that radio-frequency lock-in amplifiers typically incorporate a square wave mixer. Contributions of only a few percent from the third, fifth or seventh harmonic are enough to severely distort the measurement. One solution is to remove the harmonics with a bandpass or low-pass filter placed between the photodiode and the lock-in.[12] However, this requires the filter to be changed with the frequency. Another option which we employ is to adjust the waveform driving the EOM until the odd harmonics are minimized while observing the frequency-domain photodiode signal in real time on an oscilloscope. We performed TDTR measurements with resonant filters at specific frequencies and verified that the results matched those performed with the waveform approach using a sine wave with a carefully chosen offset and amplitude.

Another important factor is the focused size of the pump and probe spots. Again using sapphire as an example, in Fig. 7 we show the sensitivity of the solution to the spot size and, for reference, substrate thermal conductivity. Both spots are taken as having a 6 μm $1/e^2$ radius. At low frequencies the sensitivity to the spot radius is nearly as large as sensitivity to thermal conductivity. We measure the focused spots using a two-axis scanning-slit beam profiler with an accuracy of better than 0.5 μm. In addition, we used a pair of cylindrical lenses to correct the ellipticity of our laser to better than 0.9. Because the mechanical stage can remain stationary during the measurement, it is not necessary to correct for the divergence of the probe beam at different delay times. As in TDTR, the total heat capacity of the deposited metal layer ($C \times$ thickness) and film quality have a strong influence on the result[11,21] and should be determined as accurately as possible with picosecond acoustics,[22] a very well-characterized deposition chamber, or a reference sample placed by the sample of interest during the deposition run.

Finally, the analysis we have presented assumes that ma-terial properties are independent of frequency over the range of the experiment. While this is usually true, for certain materials such as semiconductor alloys such as SiGe and InGaAs, there may be a reduction in thermal conductivity at frequencies as low as 1 MHz.[23] In these cases, options include reducing the upper frequency limit of the measurement, incorporating a frequency-dependent thermal conductivity into the model, or using a time-domain approach such as TDTR to determine the thermal conductivity at specific frequencies.

VI. SUMMARY

A FDTR method has been presented for measuring thermal properties of homogenous samples and thin films, using the same spot geometry and data analysis approach as TDTR but with frequency instead of time as the changing experimental parameter. The method can simultaneously determine the thermal conductivity and heat capacity of a sample, provided the thermal diffusivity is $\gtrsim 3 \times 10^{-6}$ m^2/s, and it can be used to simultaneously measure both in-plane and cross-plane thermal conductivities. Two possible setups for FDTR were presented: one based on a pulsed laser that allows fast switching to time-domain thermoreflectance and one based on cw lasers that is simpler and less expensive. An analysis of the method's sensitivity to various properties and potential sources of error was provided and sample results were presented demonstrating good agreement with literature values.

[1] A. Mandelis, Rev. Sci. Instrum. **57**, 617 (1986).
[2] A. Rosencwaig, J. Opsal, W. L. Smith, and D. L. Willenborg, Appl. Phys. Lett. **46**, 1013 (1985).
[3] G. Langer, J. Hartmann, and M. Reichling, Rev. Sci. Instrum. **68**, 1510 (1997).
[4] A. Yarai and T. Nakanishi, Rev. Sci. Instrum. **78**, 054903 (2007).
[5] J. Opsal, A. Rosencwaig, and D. L. Willenborg, Appl. Opt. **22**, 3169 (1983).
[6] E. T. Ogawa, C. Hu, and P. S. Ho, J. Appl. Phys. **86**, 6018 (1999).
[7] B. Li, J. P. Roger, L. Pottier, and D. Fournier, J. Appl. Phys. **86**, 5314 (1999).
[8] B. Li, L. Pottier, J. P. Roger, D. Fournier, and E. Welsch, Rev. Sci. Instrum. **71**, 2154 (2000).
[9] D. Fournier and C. Fretigny, Eur. Phys. J. Spec. Top. **153**, 69 (2008).
[10] C. A. Paddock and G. L. Eesley, J. Appl. Phys. **60**, 285 (1986).
[11] W. S. Capinski, H. J. Maris, T. Ruf, M. Cardona, K. Ploog, and D. S. Katzer, Phys. Rev. B **59**, 8105 (1999).
[12] D. G. Cahill, Rev. Sci. Instrum. **75**, 5119 (2004).
[13] S. Huxtable, D. G. Cahill, V. Fauconnier, J. O. White, and J.-C. Zhao, Nature Mater. **3**, 298 (2004).
[14] A. J. Schmidt, M. Chiesa, X. Chen, and G. Chen, Rev. Sci. Instrum. **79**, 064902 (2008).
[15] A. J. Schmidt, X. Chen, and G. Chen, Rev. Sci. Instrum. **79**, 114902 (2008).
[16] W. S. Capinski and H. J. Maris, Rev. Sci. Instrum. **67**, 2720 (1996).
[17] B. C. Gundrum, D. G. Cahill, and R. S. Averback, Phys. Rev. B **72**, 245426 (2005).
[18] Y. Touloukian, *Thermophysical Properties of Matter* (Purdue University, West Lafayette, IN, 1970).
[19] J. H. Lienhard IV and J. H. Lienhard V, *A Heat Transfer Textbook* (Phlogiston, Cambridge, MA, 2005).
[20] R. M. Costescu, M. A. Wall, and D. G. Cahill, Phys. Rev. B **67**, 054302 (2003).
[21] D. G. Cahill and F. Watanabe, Phys. Rev. B **70**, 235322 (2004).
[22] C. Thomsen, H. T. Grahn, H. J. Maris, and J. Tauc, Phys. Rev. B **34**, 4129 (1986).
[23] Y. K. Koh and D. G. Cahill, Phys. Rev. B **76**, 075207 (2007).